Measurement of the five-parameter grain boundary distribution from planar sections

Gregory S. Rohrer[+] and Valerie Randle*

[+]Department of Materials Science and Engineering, Carnegie Mellon University, Pittsburgh, PA 15213-3890, USA.

*Materials Research Centre, School of Engineering, Swansea University, Swansea SA2 8PP, UK.

10.1 Introduction: grain boundary planes and properties

Although EBSD is essentially a surface measurement technique, strategies have been developed to extend its capabilities to the characterisation of microstructure in three dimensions. These developments have been able to be realised because of advances in both EBSD technology and computing power have rendered the collection of large data sets a routine matter. There are several scientific motivations for characterizing the three-dimensional structure of polycrystals by EBSD. In this Chapter, we describe the application of EBSD to the measurement of internal interface planes by application of both serial sectioning and also a stereological technique known as the 'five-parameter analysis'.

An interface (referred to as a grain boundary where it exists between crystals of the same phase) has five geometric degrees of freedom. Usually, three independent parameters are used to describe the misorientation between grains and two independent parameters describe the orientation of the boundary plane (Wolf and Lutsko 1989). Whereas the misorientation is accessed readily by EBSD performed on a single section through the specimen, the boundary plane orientation is not so readily available because the boundary surface itself is buried. Furthermore a single grain boundary, having by definition a fixed misorientation, usually consists of many differently oriented boundary plane segments, as illustrated on Fig. 1. For these reasons measurement of boundary plane crystallography has

tended to be neglected. However, both atomistic simulations and a slowly increasing amount of experimental evidence demonstrate that the boundary plane crystallography has a fundamental influence on grain boundary properties such as energy, mobility, corrosion resistance and segregation (Randle 1997). A few modern examples which demonstrate these links are:

- The effect of grain boundary orientation on energy has been illustrated in NiAl (Amouyal et al. 2005). The boundary energy was found to vary with inclination, and twist boundaries had higher energies than tilt boundaries. The data were obtained from 43 grain boundaries via a combination of EBSD, serial sectioning, thermal grooving and scanning probe microscopy.
- In directionally solidified pure copper it was found that the corrosion resistance of grain boundaries was correlated to the interplanar spacing at the boundary, but not the Σ-value, for [110] tilt boundaries (Miyamoto et al. 2004). This work was carried out on 26 grain boundaries in tricrystals, by X-ray back reflection Laue diffraction combined with atomic force microscopy measurements on corrosion grooves.
- In bicrystals of an Fe-Si alloy grain boundaries with [100] tilt misorientations, symmetric tilt boundaries and asymmetric boundaries formed with a (110) plane were found to be resistant to segregation (Lejcek et al. 2003).
- Studies of grain boundary wetting by liquid copper in an iron alloy indicated that the propensity for wetting increased with the grain boundary free volume and the atomic roughness of the surfaces comprising the boundary (Wynblatt and Takashima 2001). The data were obtained by EBSD and serial sectioning from 975 boundaries.
- A different experimental approach to the study of grain boundary planes is to adapt EBSD to measure the indices of intergranular fracture surfaces. Using this method it was found that in TiO_2 there was reduced segregation to low energy boundary planes (Pang and Wynblatt 2005).

Boundaries which have improved properties compared to those of a random boundary have come to be known as ‘special’ boundaries. It used to be thought that special boundaries were low-Σ

coincidence site lattice (CSL) boundaries. Now it is realised that the orientation of the boundary plane has a greater influence on properties than does the misorientation (Rohrer et al. 2004).

10.2 Serial sectioning

Unless the component grain boundaries in a specimen have a predefined or easily measurable geometry, such as bicrystals, tricrystals, columnar grains, thin films, fracture surfaces etc., a serial sectioning procedure has in the past been used to obtain the orientation of the boundary plane. Figure 2 illustrates the parameters required to specify the orientation of a single boundary plane. The sample reference frame is *xyz*, the grain boundary trace vector on the specimen surface is $\boldsymbol{l'}_{ij}$, the grain boundary plane normal is $\boldsymbol{n'}_{ij}$, the 'trace angle' and the 'inclination angle' as illustrated on Fig. 2 are α and β respectively, and the section depth is t. Also required is a means of calibrating accurately the depth of section removed and ensuring accurate registration between successive sections. If these parameters are obtained manually, data sets tend to be small because these operations are tedious. In the 1990s information on the crystallographic indices of planes from several metals was obtained (Randle 1995, 1997).

More comprehensive analysis of serial section data has made it possible to determine the inclinations of many thousands of grain boundaries and, therefore, determine the five-parameter grain boundary character distribution (GBCD) (Saylor et al. 2003, 2004a). Each grain boundary trace on a two dimensional section plane is approximated by a series of short tangent lines. When traces from the same interfaces are located on two adjacent layers, the interface can be represented by a series of triangles joining two pixels on one layer with a third pixel on an adjacent layer, as illustrated in Fig. 3. The normal of each triangle is therefore known and as long as the grain orientations have been measured by EBSD, it is also possible to determine the misorientation. With information from a sufficient number of triangles, the GBCD can be calculated.

10.3 Single-surface trace analysis

More recently, interest has been generated in exploiting the information provided from the grain boundary trace direction on the specimen surface, and dispensing with the serial sectioning step. This is because there are unavoidable geometrical errors involved in serial sectioning and three dimensional reconstruction. For example, the assumption has to be made that the interface is parallel within the section depth. These errors are an order of magnitude greater than errors in a single section plane. Serial sectioning is also laborious and time consuming.

The crystallographic boundary trace direction plus the misorientation between neighbouring grains provides four out of the five boundary parameters. The 'trace vector' $\boldsymbol{l'}_{ij}$ (Fig. 2) can be calculated, from EBSD data, in the coordinate systems of both interfacing grains, where it is referred to as $\boldsymbol{l}_{ij}$ (note that throughout this chapter, primed vectors denote the sample reference frame and unprimed vectors denote the crystal frame). Because $\boldsymbol{l}_{ij}$ lies in the grain boundary plane it is orthogonal to the boundary plane normal vector $\boldsymbol{n}_{ij}$ and it must be true that $\boldsymbol{l}_{ij} \bullet \boldsymbol{n}_{ij} = 0$. This condition can be used to check if the boundary plane normal could be <111>, for example, in one or both grains. If $\boldsymbol{l}_{ij} \bullet <111> \neq 0$, then the boundary cannot be {111}. On the other hand if $\boldsymbol{l}_{ij} \bullet <111> = 0$, then the boundary plane might be on {111}. If the condition applies in both interfacing grains, then it is likely that the boundary is either a coherent twin (if the boundary is a Σ3) or a {111} twist boundary (if the boundary has some other misorientation about [111]). This calculation therefore supplies valuable information about the boundary plane crystallography: what the plane cannot be and what it is likely to be (Randle, 2001). In previous work where the method was rigorously tested and validated, for Σ3 boundaries analysed in brass, only 10% of the cases were ambiguous in terms of recognising the type of Σ3 (coherent or incoherent) by the single-surface trace analysis compared to a full serial sectioning analysis (Randle and Davies, 2002).

The methodology for identifying the possibility of twinning in this way has been automated by use of an algorithm which extracts the boundary trace position from EBSD orientation maps. This algorithm has been used to investigate twinning in zirconium, nickel

and copper (Wright and Larsen, 2002) and to study the relationship between precipitate-free zone width and grain boundary type in an aluminium alloy (Cai et al. 2007). More significantly, it is used as part of the procedure to determine automatically all five boundary parameters from a single section (see Section 10.4)).

The automated boundary trace reconstruction routine works on an orientation map in which grains have been identified as groups of similarly oriented points, from which grain boundaries are defined according to a pre-set tolerance. Triple junctions can then be located and a first attempt at reconstructing a boundary trace is made by joining the two neighbouring triple junctions, as shown in Fig. 4a. However the grain boundary is rarely a straight line between the two junctions, and so the reconstructed trace needs to be segmented to follow more closely the true boundary. This is done by locating the point on the true boundary furthest from the reconstructed boundary. If the perpendicular distance between this point and the reconstructed boundary exceeds a predefined tolerance, then the reconstructed boundary is split into two line segments, as shown on Fig. 4b. This procedure is repeated until all points on the reconstructed boundary are within the tolerance distance of the true boundary.

Figure 4c shows a small map wherein reconstructed boundaries are superimposed on true boundaries. To minimise errors, a small step size needs to be used to generate the EBSD map in order to reproduce the boundary positions as faithfully as possible, given the discrete nature of the measurement grid. Then the segmenting process must aim to reproduce the true boundary rather than any 'noise' on the boundary length. It is therefore essential that a small tolerance, e.g. twice the map step size, is chosen to reconstruct boundaries. The expected error for a boundary of length six times greater than the scan step size would be ± 2° (Wright and Larsen, 2002). Finally, an average orientation from each neighbouring grain is associated with each segment of the reconstructed boundary trace. Measurement points between one and five steps from the boundary are used in the averaging.

10.4. Five-parameter stereological analysis

10.4.1. Parameterization and discretization of the space of grain boundary types

For evaluation of the five-parameter GBCD, we choose lattice misorientation (Δg) and grain boundary plane orientation ($\boldsymbol{n}$) to parameterize the function $\lambda(\Delta g,\boldsymbol{n})$, which is the relative areas of grain boundaries within a polycrystal distinguished by Δg and $\boldsymbol{n}$. For all of our calculations, we parameterize the lattice misorientation using three Eulerian angles ϕ_1, Φ, and ϕ_2. However, for display of the data, we choose the angle/axis system θ/[uvw], which is more intuitive. The grain boundary plane orientations are parameterized using spherical angles θ and ϕ in both the calculations and the display of the data. In the complete domain, these five angular parameters, ϕ_1, Φ, ϕ_2, θ, and ϕ range from 0 to 2π, π, 2π, π, and 2π, respectively. For most crystal systems, this complete domain contains many indistinguishable, symmetrically related parameter configurations. Therefore, one can choose a sub-domain that reduces some of the degeneracy in the calculations. In our calculations, we use a sub-domain in which the misorientation parameters range from zero to $\pi/2$, $\pi/2$, and $\pi/2$ for ϕ_1, Φ, and ϕ_2 respectively. This sub-domain is 1/64th of the entire range of possibilities and is a convenient choice because it is the smallest volume that contains an integer number of fundamental zones and can still be partitioned in a simple way. For the cubic system, there are 36 general equivalent grain boundaries for any particular set of parameters in the sub-domain.

To partition the misorientation sub-domain into cells of equal volume, we equally partition ϕ_1, $\cos(\Phi)$, and ϕ_2. In this case, there are D^3 cells with $\Delta\phi_1 = \Delta\phi_2 = \pi/2D$ and $\Delta\cos\Phi = 1/D$. The cells in Euler space can be visualized as a three dimensional rectangular parallelepiped, as illustrated in Fig. 5a. For each cell in the misorientation space, there is also a distribution of grain boundary normals, $\boldsymbol{n}$. For centrosymmetric crystals, the two spherical angles (θ and ϕ) in the range between 0 and $\pi/2$ and 0 and 2π, respectively, reproduce the domain of $\boldsymbol{n}$ (it is assumed to have a center of sym-

metry and only the upper hemisphere of surface orientation space is considered). So that each cell has the same area on the surface of a unit sphere, the domain of $\boldsymbol{n}$ is parameterized by $\cos\theta$ and ϕ, as illustrated in Fig. 5b. If there are D cells for every $\pi/2$ radians, then there will be a total of $D \bullet 4D$ cells, each with the size $\Delta\cos\theta = 1/D$ and $\Delta\phi = 2\pi/4D$. With the five dimensional grain boundary parameter space divided into cells of equal volume, each cell has the same probability of being populated by a random choice of parameters.

Based on the parameterization described above, there $4D^5$ equal volume cells in the sub-domain. The appropriate resolution for the five dimensional space should lie in the range between 5° and 10°. The rational for this is that grain boundary properties are known to vary over intervals smaller than 10 °, but measuring grain boundary plane orientations with an accuracy greater than 5° is probably not realistic. With a resolution of 5°, D = 18 and with 10°, D = 9 and for these choices, there are 7.5×10^6 and 2.4×10^5 cells in the sub-domain. For the cubic case, the number of distinguishable cells is 2.1×10^5 and 6.5×10^3, respectively. This provides guidance for the number of observations required to reliably determine the GBCD. Because the number of distinguishable bins at 5° resolution is 32 time that at 10°, many more observations are needed at higher angular resolution.

10.4.2. Measurement of the GBCD

Stereological measurements of $\lambda(\Delta g, \boldsymbol{n})$ begin with a set of boundary trace vectors, $\boldsymbol{l'}_{ij}$, defined as the trace where the j^{th} boundary tangent plane on the i^{th} grain meets the surface. Traces on a real micrograph are shown on Fig. 4c and the geometry of a single trace is represented schematically in Fig. 6a. While each $\boldsymbol{l'}_{ij}$ can be associated with a specific misorientation in the five-parameter space, $\boldsymbol{n'}_{ij}$ is not well defined. However, as implied above in the section 10.3 on the analysis of twin boundaries, it must be true that the actual grain boundary plane belongs to a set of planes that includes the surface trace and obeys the condition $\boldsymbol{l'}_{ij} \bullet \boldsymbol{n'}_{ijk} = 0$, where the vectors $\boldsymbol{n'}_{ijk}$ are a set of C unit normals to the possible grain boundary planes

(see Fig. 6b). Therefore, each observed trace can be used to generate a set of vectors perpendicular to possible boundary planes that can be transformed to the crystal reference frame (see Fig. 6c). With knowledge of the misorientation, the vectors $\boldsymbol{n}_{ijk}$ specify C cells into which $|\boldsymbol{l}_{ij}|$ are added so that the observations are weighted by line length. In other words, the length of each observed trace is counted C times. In the end, we would like to know the fractional length of line segments crossing each plane, since this is equal to the fractional area of each plane.

If there are N observations of traces from indistinguishable bicrystals, then we can be certain that for this misorientation, we have accumulated N correct boundary normal orientations and $N(C-1)$ incorrect assignments. It is worth noting that the bicrystals sampled should have a random orientation distribution with respect to the sample reference; preferred orientations bias the distribution and will lead to unreliable results. To get the line length crossing each boundary type, we have to remove the incorrect assignments. To do this, it must be realized that the incorrect assignments are not distributed randomly. If there is a peak in the real distribution of grain boundary planes, then orientations very close to this pole will have more incorrectly assigned length than others. This is because these neighboring cells have a greater probability of being in the zone of the peak orientation than an orientation further away. Conversely, orientations far from the maximum are less likely to share a zone with the most highly populated orientation and will accumulate less incorrectly assigned length. By making an approximation for this inhomogeneous distribution, it is possible to subtract the incorrectly assigned lengths. This procedure has been described in detail elsewhere (Saylor et al. 2004b).

When using this stereology to make GBCD measurements, the factors that influence the accuracy are the discretization for the parameters, the accuracy of the line segment orientations, and the number of observations. The discretization of the system influences the discrimination of closely spaced features in the distribution and the magnitudes of the peaks. If, for example, there are two peaks separated by less than the spacing of the cells, they will be merged to a single peak. Features that are sharper than the cell size will also be broadened and have reduced intensity. The discretization also in-

fluences how the peak values are interpreted. For example, the upper limit of the population, measured in MRD, is equal to the number of distinguishable cells (this can be reached only when all of the observations fall into a single cell). For example, in a cubic system with D=9 (cell size of approximately10 °), there are 6561 distinguishable cells. It was recently reported that with D=9, the peak of the distribution for a Ni specimen occurred with a value of 1428 MRD at the position of the coherent twin (Randle et al. 2008b). This implies that at least 22% (1428/6561) of the grain boundary area is made up of coherent twins. Because the distribution of coherent twins is expected to be narrower than the 10° cell size, the actual fractional boundary area may be larger. For the remainder of the discussion, we will focus on cubic systems in with a 10° (D=9) cell size.

10.4.3. Performance of the stereological analysis

The agreement between the stereologically measured distribution and a true (simulated) distribution has been shown to depend on the number of observations. If only 10^4 grain boundary traces are used, then there are errors of greater than 0.5 MRD (multiples of a random distribution) in a large fraction of the cells (see Fig. 7). However, if $2.5x10^5$ boundaries are measured, then less than 1 % of the cells have an error this large. If $5x10^4$ traces are used, fewer than 5 % of the cells have errors greater than 0.5 MRD. Balancing the desire for accuracy against the time required to make the observations, it was concluded that $5x10^4$ traces are sufficient and this standard has been used the in the majority of the work that has followed (Saylor et al. 2004b). However, it must be noted that the errors are most likely to occur at the maxima in the distributions and it is frequently these maxima that are interpreted. In comparative studies, it is essential to understand how different two distributions need to be before it can be concluded that they are actually different. This question has been addressed by simulations and these results are described in the remainder of this section.

In simulating experimental observations, it is important to recognize that the boundary traces are not permitted to have a con-

tinuous range of orientations in the sample reference frame. Because of the discrete nature of the EBSD map, the end points of grain boundary traces are confined to the nodes of a two dimensional honeycomb lattice. The relevant scale for this is the ratio of the EBSD step size to the average grain diameter. The allowed ranges of orientation become more continuous as the grain size to pixel ratio increases.

Simulations were carried out to determine how the number of observations and the grain size to pixel ratio influence the observed distribution of grain boundary planes. To begin, a model GBCD was designed to mimic the distribution observed for $SrTiO_3$ (Saylor et al. 2004). The GBCD has a small enhancement of low angle grain boundaries and peaks at the positions of {100} planes. The value of each cell was defined by its proximity to the misorientation of 2° about [100] and to the {100} grain boundary plane orientation. For each type of boundary, the amplitude of the GBCD (A) was given by the combination of a misorientation determined component (A_1) and a grain boundary plane determined component (A_2).

$$A = A_1+(A_2 \bullet A_1) \qquad (10.1)$$

The misorietation determined component is:

$$A_1 = 1 + A_m \exp[-(\theta_m/W_m)^2] \qquad (10.2)$$

Where A_m=1.5, θ_m is the disorientation between the current cell and the 2°/[100] misorientation, and W_m, the width of the distribution, is 10°. This leads to an MDF that has a weak maximum for low misorientation boundaries and is constant elsewhere. The grain boundary plane orientation determined component of the amplitude is given by:

$$A_2 = A_o \exp[-(\theta_o/W_o)^2] \qquad (10.3)$$

Where A_o=400, θ_o is the angle between the normal to {100} and the plane of interest. W_o, the width of the distribution, is 10°.

This distribution was used to generate simulated data in the following way. First, a random misorientation and grain boundary plane orientation were selected. If they are consistent with the dis-

tribution, the observation is kept and if not, it is discarded and another is selected. Whenever an observation is kept in the distribution, a random direction within the grain boundary plane is selected (to simulate the observation of a boundary trace). At this point, the domain of trace orientations is continuous. To simulate the effect of the grid, the closest line segment on a finite, 2D hexagonal lattice is selected and this is saved as a simulated observation. The process is repeated as many times as necessary to generate simulated data and can then be used to determine the GBCD.

To test the influence of the number of line segments on the extreme points in the distribution, simulation data sets containing $5x10^3$, $1x10^4$, $2.5x10^4$, $5x10^4$, $1x10^5$, $2.5x10^5$, and $5x10^5$ traces were created and the GBCD was calculated. For these simulations, the grain size to pixel ratio was 50, which is assumed to closely approximate a continuous distribution and eliminate this factor from the analysis. The distribution of grain boundary planes at the misorientation of 45 ° about the [100] axis was selected as a characteristic example. The results in Fig. 8 show the maximum and minimum of the distribution as a function of the number of traces and the grain boundary plane distribution for three cases. Note that the reference frame defined in the caption is used throughout this chapter. If the distribution determined from $5x10^3$ segments is excluded, then the average of maxima is 3.25 MRD with a standard deviation of 0.3 MRD, or about 10 % of the maximum. While the value of the maximum determined from $1x10^4$ traces is within 10 % of that determined from larger number, it is also clear that not all features in the distribution are represented. Specifically, the peaks along the vertical axis, corresponding to tilt boundaries, are not reproduced. The distribution from $5x10^4$ traces, on the other hand, is nearly the same as the one from ten times as many segments. We therefore conclude that $5x10^4$ traces are sufficient to reproduce the distribution.

One can also ask how reproducible the values of the peak positions are. When four different randomly generated sets of data were analyzed, each containing $5x10^4$ line segments, the peak for the distribution of planes for a misorientation of 45° about [100] ranged from 2.76 MRD to 3.33 MRD. The four values had an average of 3.10 MRD and a standard deviation of 0.27 MRD. Therefore, we

conclude that the maxima of the distribution are reproducible within a range of about 10 %.

To examine the effect of the step size, we consider a constant set of $5x10^4$ traces, confined to 2D, SxS, hexagonal lattices where S = 3, 5, 10, and 50. The results shown in Fig. 9 illustrate that there is a negligible difference in the maxima for the distributions determined with 10 and 50 steps per grain diameter. Furthermore, the shapes of the distributions at these two lattice resolutions are nearly identical. Based on this, we conclude that 10 orientation points per grain diameter is sufficient to determine the distribution and that fewer lattices points will lead to underestimates of the maxima.

The results of the simulations described above allow us to provide some practical guidelines for the acquisition and analysis of the EBSD data used to determine the GBCD. The first is that the resolution of the EBSD mapping should be at least 10 points per grain diameter. The second point is that when comparing two GBCDs, differences of less than 10 % should be considered insignificant. The third is that at least $5x10^4$ grain boundary traces should be recorded to determine the GBCD. This estimate assumes that they are relatively evenly distributed. Note that if too many of the segments arise from a single type of misorientation, then there will be grain boundary configurations that are not sampled. For example, if one third of all the boundaries are coherent twins, then $1.7x10^4$ traces will fall in one cell and $3.3x10^4$ will distributed among the remaining 6560 cells. While the grain boundary plane distribution will be well determined for the twin misorientation, it will be underdetermined for all of the other misorientation types.

10.4.4. Comparison GBCDs measured stereologically and by serial sectioning in the Dual Beam FIB

Recently, the dual-beam focused ion beam (FIB) scanning electron microscope (SEM) has been used to automate the collection of serial sections of electron backscatter diffraction maps (Konrad et al. 2006; Uchic et al. 2006). Determining the GBCD from such data has been accomplished only recently (Dillon and Rohrer 2008). One of the principle challenges of determining the GBCD from 3D orien-

tation data is the voxelization of the interfaces which leads to discrete boundary orientations in the sample reference frame. One approach to this problem is to use the grain boundary traces, extracted from the individual layers as described in the previous section. After complementary segments have been identified on adjacent layers, the two end points from one layer and one of the end points from an adjacent layer can be used to form triangular areas that represent the grain boundary. These areas are classified according to their lattice misorientations and grain boundary plane orientations as described above. This approach gives results that are similar to the results of the stereological analysis. This is demonstrated in Fig. 10, which shows the distribution of grain boundary planes for the Σ3 (60°/[111]) grain boundary in Y_2O_3 derived by the two techniques. Both methods produce peaks at the position of the (111) twist boundary and are therefore qualitatively similar, but there is a quantitative difference in the intensity. The origin of the difference in the quantitative results is currently being investigated.

10.5. Examples of five-parameter analyses

The five-parameter analysis has been used to measure the misorientation and grain boundary plane distributions of a number of materials and processing variants. These include a range of ceramics, e.g. MgO, NaCl, $SrTiO_3$, TiO_2, WC, $MgAl_2O_4$ (Saylor et al. 2003, 2004a, 2004c; Pennock et al. 2008; Pang and Wynblatt 2005; Kim et al. 2008) and metals, e.g. Al, Cu, Ni, brass, austentitic steels, Ti (Saylor et al. 2004d; Randle et al. 2006, 2008a, 2008b; Downey et al. 2007; Jones et al. 2008). We will describe some of these as illustrations of the five-parameter analysis technique.

The five-parameter grain boundary distribution has been measured on a slightly deformed NaCl (rocksalt) specimen which contained a small quantity of intergranular brine (Pennock et al. 2008). This specimen was of interest because in planar sections the NaCl specimen featured distinct square shaped grains for a wide range of deformation and annealed conditions. A study of grain boundary traces using EBSD showed that the traces of the square shaped grains were within 12º of the trace of {100} planes (Pennock

et al. 2006). Figure 11 shows a plot of the distribution of boundary planes for the entire sample population, as measured by the five-parameter method. There are peaks at {100}. More information on the distribution of planes is gleaned if sections through the five-parameter space are viewed. For the NaCl distribution low-index, high symmetry misorientation axes [100], [110] and [111] were chosen in addition to [123], which was chosen to represent a low symmetry axis. Figure 12 shows the 20° misorientation angle section for these four axes. The misorientation axis is marked on each plot in Fig. 12. For each misorientation there are distinct peaks, with maxima for the planes distribution in the range 3.5-4.2 MRD.

In Fig. 12a there are both twist boundaries and asymmetric tilt boundaries along the (100) zone. The distribution of planes along the (100) zone shows that one of the interfacing planes is (100) and the counterpart plane in the neighbouring grain is 20° displaced (which it is geometrically required to be) on the (100) zone. The 20°/[110] misorientation section shows no twist or asymmetrical tilt boundaries (Fig. 12b). Rather, the planes are close to {100}, with some spread indicating the presence of the geometrical counterpart to the {100} plane on the other side of the interface. A similar result is seen for the 20°/[111] and 20°/[123] sections. It is clear that in these data there is a very strong propensity for {100} boundary planes. Previous five-parameter data collected from MgO, using the serial sectioning method, showed similar trends to the data for NaCl (Saylor et al. 2003).

Figure 13 shows an example of the five-parameter analysis performed on an alloy with a hcp crystal structure, Ti-6%Al-4%V (Randle et al. 2008a). The alloy had been deformed 10% by cold rolling, and therefore contained deformation twins. Figure 13a shows the planes distribution in the deformed specimen for Σ13b, 57.4°/[$2\bar{1}\,\bar{1}0$]. There is a single, very pronounced maximum of 120 MRD located at the $(01\bar{1}1)$ plane. It corresponds to the $\{10\bar{1}1\}$ $<\bar{1}012>$ twin system of the Σ13b CSL, which is the deformation twin. Figure 13b shows the same distribution after annealing. The peak associated with the plane of the deformation twin has decreased marginally.

The five-parameter stereology has been applied extensively to fcc metals and alloys. An example is shown here of annealed cop-

per. Figure 14a shows the distribution for all boundaries. There is a strong peak at {111} which is largely due to the presence of many coherent annealing twins, where the habit plane is {111}. 61% of the total interface length was Σ3. However, when all Σ3 boundaries are removed from the data set (Fig. 14b), there is still a small peak at {111}, with a value of 1.36 MRD. Figure 15 shows the planes distribution for the <110> misorientation axis, for the entire misorientation angle range (10°-60°). The planes of high angle boundaries are mostly spread along the (110) zone, i.e. they are [110] asymmetrical tilt boundaries. The maxima have high MRD values, especially in the 30° and 40° sections, which correspond to Σ27 and Σ9 boundaries respectively. These boundaries are generated as a result of multiple twinning. Figure 16 shows the planes distribution for the [111] misorientation axis. On the whole there is a tendency for (111) twist boundaries to predominate, i.e. there are maxima at (111). In both Fig. 15 and Fig. 16, Σ3 boundaries have been omitted. The planes distribution for the [100] misorientation axis is not presented here because plane densities with values of only one MRD or less were recorded.

There are some striking similarities between all the fcc metals examined so far; for example, the overall planes distribution is always dominated by {111}, even when Σ3 misorientations have been extracted. Also, there are some significant differences depending on the processing route and specific material parameters (Randle 2006, 2008b). The five-parameter data acquired has contributed to our knowledge and understanding of grain boundaries in polycrystals. In particular, the analysis of these and previous results from ceramic materials has led to the suggestion that ‘special’ boundaries are those which terminate on low-index boundary planes (Rohrer et al. 2004). This is in contrast to previous, misorientation-based definitions of a special boundary.

10.6. Acknowledgement

The work at Carnegie Mellon University was supported primarily by the MRSEC program of the National Science Foundation under Award Number DMR-0520425. The work at Swansea was partially supported by the Engineering and Physical Sciences Research Council.

10.7. References

Amouyal, Y., Rabkin, E., and Mishin, Y., 2005, Correlation between grain boundary energy and geometry in Ni-rich NiAl, *Acta Mater*. 53:3795

Cai, B., Adams, B.L., and Nelson, T.W., 2007, Relation between precipitate-free zone width and grain boundary type in 7075-T7 Al alloy, *Acta Mater*. 55:1543.

Dillon, S., and Rohrer, G.S., 2008 Grain Boundary Plane distributions in ceramics derived from three-dimensional orientation maps, *J. Amer. Ceram. Soc.*, in preparation.

Downey, II, S.T., Bembridge, N., Kalu, P.N., Miller, H.M., Rohrer, G.S., Han, K., 2007, Grain Boundary Plane Distributions in Modified 316 LN Steel Exposed at Elevated and Cryogenic Temperatures, *J. Mater. Sci.*, 42:9543.

Jones, R., Owen, G., and Randle, V., 2008, Carbide precipitation and grain boundary plane selection in overaged type 316 austenitic stainless steel, *Mater. Sci. Eng,* in press.

Kim, C.-S., Massa, T.R., Rohrer, G.S., 2008, Interface character distributions in WC-Co composites, *J. Am. Ceram. Soc.* 91:996.

Konrad, J., Zaefferer, S., and Raabe, D., 2006, Investigation of orientation gradients around a hard Laves particle in a warm-rolled Fe_3Al-based alloy using a 3D EBSD-FIB technique, *Acta Mater.* 54:1369.

Lejcek, P., Hofmann, S. and Paidar, P., 2003, Solute segregation and classification of [100] tilt grain boundaries in α-iron: consequences for grain boundary engineering, *Acta Mater*. 51:3951.

Miyamoto, H., Ikeuchi, K., and Mimaki, T., 2004, The role of grain boundary plane orientation on intergranular corrosion of symmetric and asymmetric [110] tilt grain boundaries in directionally solidified pure copper, *Scripta Mater.* 50:1417.

Pang, Y., and Wynblatt, P., 2005, Correlation between grain-boundary segregation and grain-boundary plane orientation in Nb-doped TiO_2, *J. Am. Ceram. Soc*. 88:2286.

Pennock, G.M., Drury, M.R., and Spiers, C.J., 2006, Grain boundary populations in wet and dry NaCl, *Mater. Sci. Tech.* 22:1307.

Pennock, G., Coleman, M., Drury, M., and Randle, V., 2008, Grain boundary plane populations in minerals; the example of wet NaCl after low strain deformation, submitted to *Contributions to Mineralogy and Petrology*.

Randle, V,. 1997, The role of the grain boundary plane in cubic polycrystals, *Acta Mater*. 46:1459.

Randle, V., 1995, Crystallographic characterisation of planes in the scanning electron microscope, *Mater. Charact*. 34:29.

Randle, V., 2001, A methodology for grain boundary plane assessment by single trace analysis, *Scripta Mater*. 44:2789.

Randle, V., and Davies, H., 2002, A comparison between three-dimensional and two-dimensional grain boundary plane analysis, *Ultramicros*. 90:153.

Randle, V., Rohrer, G., Kim, C., and Hu, Y, 2006, Changes in the five-parameter grain boundary character distribution in alpha-brass brought about by iterative thermomechanical processing, *Acta Mater*. 54:4489.

Randle, V., Rohrer, G., and Hu, Y., 2008a, Five-parameter grain boundary analysis of a titanium alloy before and after low temperature annealing, *Scripta Mater*. 58:183.

Randle, V., Rohrer, G.S., Miller, H.M, Coleman, M., and Owen, G.T., 2008b, Five-parameter grain boundary distribution of commercially grain boundary engineered nickel and copper, *Acta Mater*., 56:2363.

Rohrer, G.S., Saylor, D.M., El Dasher, B., Adams, B.L., Rollett, A.D., and Wynblatt, P., 2004, The distribution of internal interfaces in polycrystals, *Zeit. Metall.* 95:197.

Saylor, D.M., El Dasher, B., Sano, T., and Rohrer, G.S., 2004a, Distribution of Grain boundaries in $SrTiO_3$ as a Function of Five Macroscopic Parameters, *J. Amer. Ceram. Soc.*, 87:670.

Saylor, D.M., El Dasher, B., Adams, B.L., and Rohrer, G.S., 2004b, Measuring the five-parameter grain-boundary distribution from observations of planar sections, *Met. Mat. Trans A* 35:1981.

Saylor, D.M., El Dasher, B., Pang, Y., Miller, H.M., Wynblatt, P., Rollett, A.D., and Rohrer, G.S., 2004c, "Habits of Grains in Dense Polycrystalline Solids," *J. Amer. Ceram. Soc.* 87:724.

Saylor, D.M., El Dasher, B., Rollett, A.D., and Rohrer, G.S., 2004d, Distribution of grain boundaries in aluminium as a function of five macrosopic parameters, *Acta Mater*. 52:3649.

Saylor, D.M., Morawiec, A., and Rohrer, G.S., 2003, Distribution of grain boundaries in magnesia as a function of five macrosopic parameters, *Acta Mater*. 51:3663.

Uchic, M.D, Groeber, M.A., Dimiduk, D.M., and Simmons, J.P., 2006, 3D microstructural characterization of nickel superalloys via serial-sectioning using a dual beam FIB-SEM, *Scripta Mater*. 55:23.

Wolf, D., and Lutsko, J.F., 1989, On the relationship between tilt and twist grain boundaries, *Zeit. Kristall*. 189:239.

Wright, S.I., and Larsen, R.J., 2002, Extracting twins from orientation imaging microscopy scan data, *J. Micros*. 205:245.

Wynblatt, P., and Takashima, M., 2001, Correlation of grain boundary character with wetting behaviour, *Interface Science* 9:265.

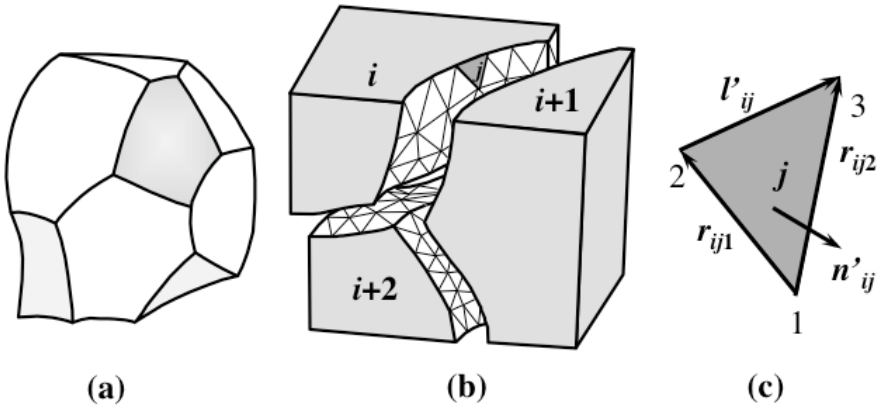

Figure 1. (a) Schematic shape of a single grain from a dense polycrystal. (b) Representation of a three grain junction within a polycrystal. The view is exploded so that the internal interfaces can be seen. The external surfaces are shaded and the internal surfaces are triangulated. The j^{th} triangular facet on the i^{th} grain is shaded and an enlarged view of this facet is shown in (c). (Rohrer et al. 2004)

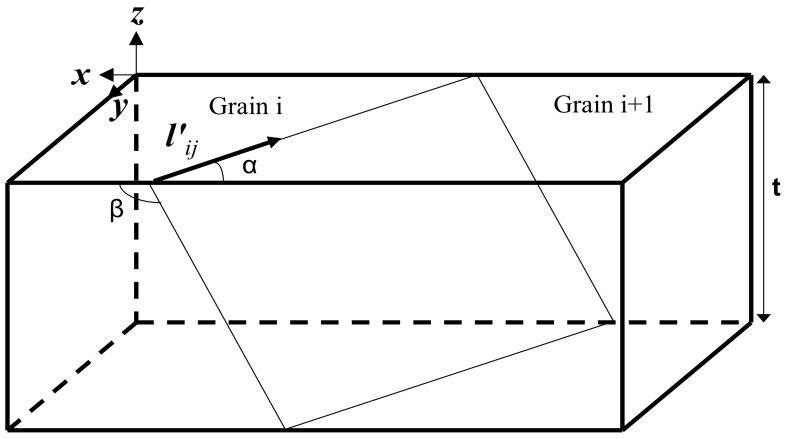

Figure 2. The parameters required to specify the crystallographic orientation of a single boundary plane (thin lines). The sample reference frame (thick lines) is *xyz* and the grain boundary trace vector on the specimen surface is $\boldsymbol{l'}_{ij}$, the 'trace angle' and the 'inclination angle' are α and β respectively, and the section depth is t.

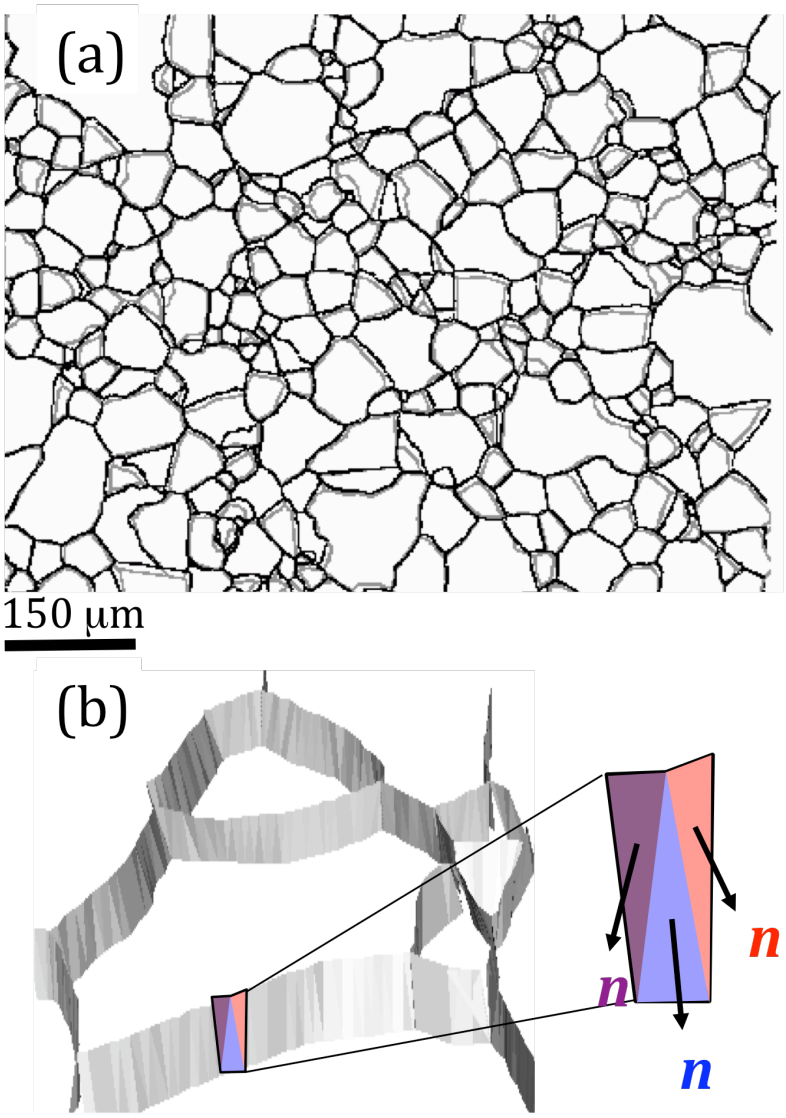

Figure 3. (a) A superposition of the grain boundary traces from adjacent layers in the microstructure of MgO. The vertical separation is about 5 μm. (b) Illustration of the formation of triangles between traces on adjacent layers, with known lattice misorientation and orientation.

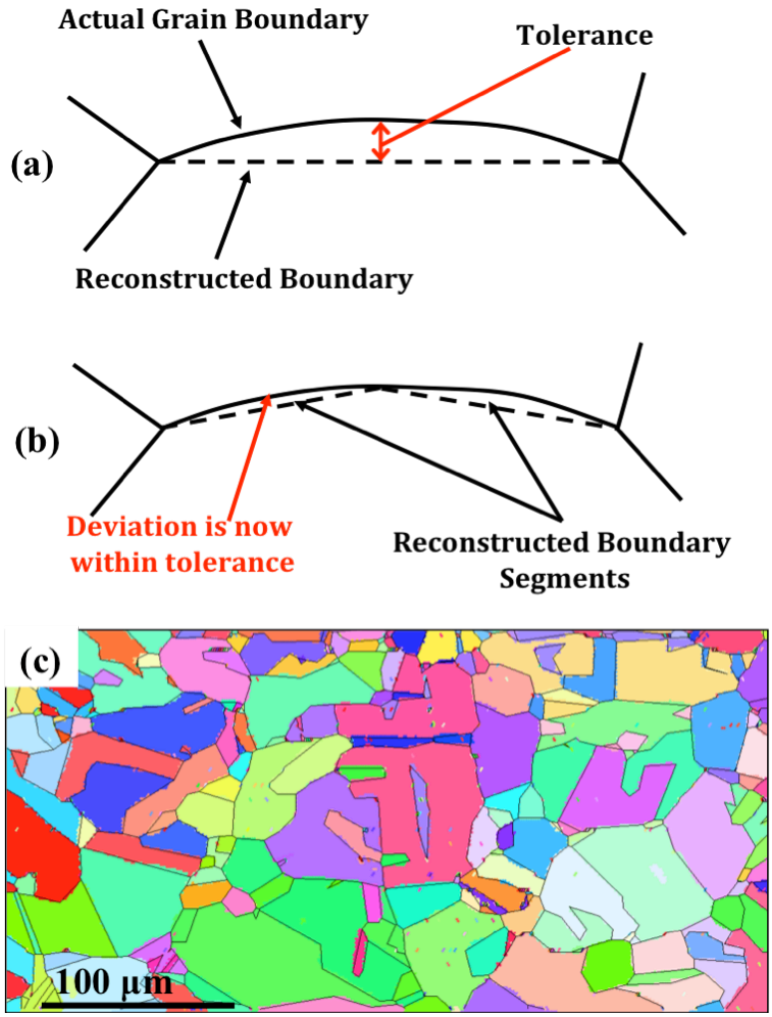

Figure 4. Illustration of the boundary trace reconstruction routine. (a) First reconstruction attempt, by joining adjacent triple junctions. (b) Segmentation of the reconstructed trace. (c) Small map wherein reconstructed boundaries are superimposed on true boundaries. Grains are coloured randomly.

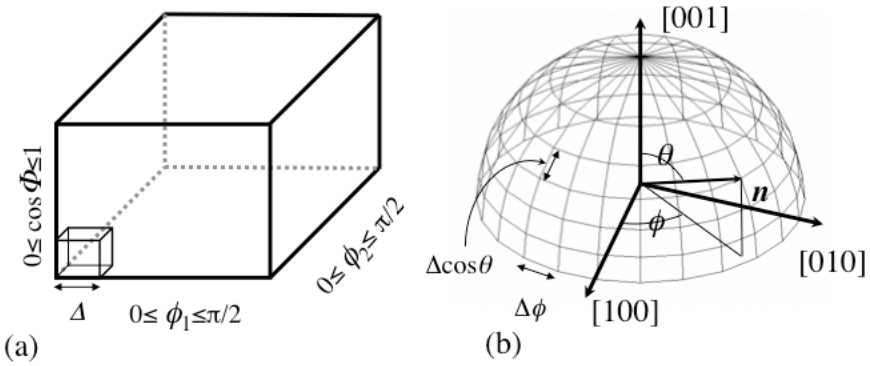

Figure 5. The parameterization of $\lambda(\Delta g, \boldsymbol{n})$ into (a) three lattice misorientation parameters and (b) two boundary plane orientation parameters. (b) Definition of the spherical angles used to parameterize $\boldsymbol{n}$. The range of $\boldsymbol{n}$ is partitioned so that all of the cells have the same width in ϕ and $\cos\theta$ and the same area on the surface of the hemisphere. In the misorientation space, there are D^3 cells and for each of these cells, there is a hemisphere of boundary plane normals with $4D^2$ cells.

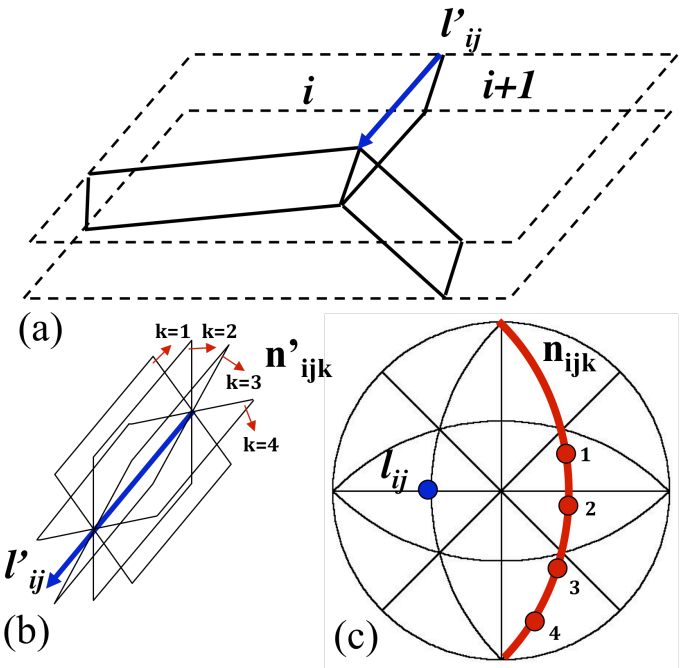

Figure 6. Schematic of interpretation of boundary traces. (a) A trace between crystals i and j in the sample reference frame is identified. (b) The grain boundary normal is one of the set $\boldsymbol{n}'_{ijk}$. (c) Represented on a stereogram in the grain boundary reference frame, the boundary trace is a point and the set of possible plane is a great circle.

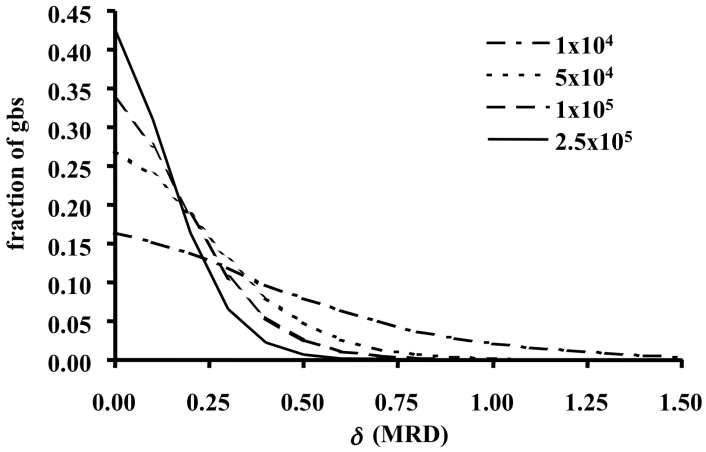

Figure 7. The distribution of the differences, δ (absolute value), between the recovered and actual GBCD from data sets consisting of $1x10^4$, $5x10^4$, $1x10^5$, and $2.5x10^5$ simulated boundaries (Saylor et al. 2004).

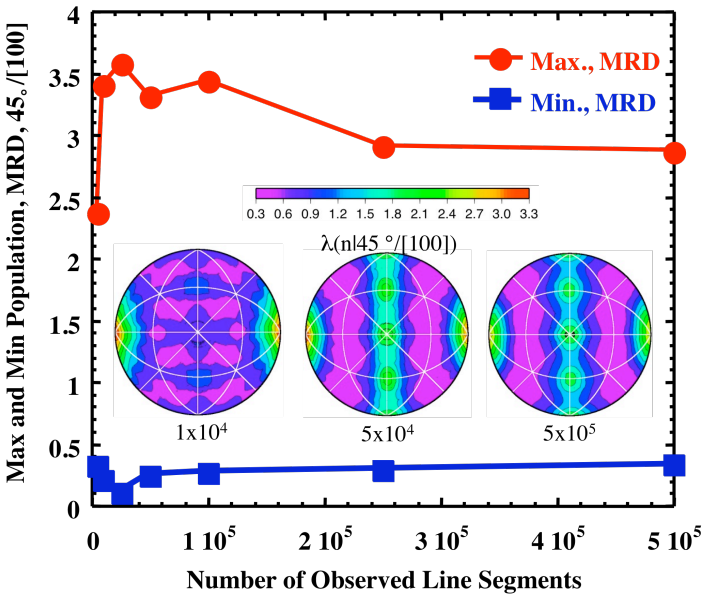

Figure 8. Results from the stereological analysis of simulated data sets comprised of varying numbers of boundary traces. The circles and squares indicate the maximum and minimum values of the distribution for the 45°/[100] misorientation and the inset shows the grain boundary plane distributions for three of the data sets. The reference frame of these an other projection in the chapter has [001] perpendicular to the plane of the paper and [100] pointing horizontally to the right. The distribution computed from $5x10^4$ traces is not significantly different from that determined from $5x10^5$ traces.

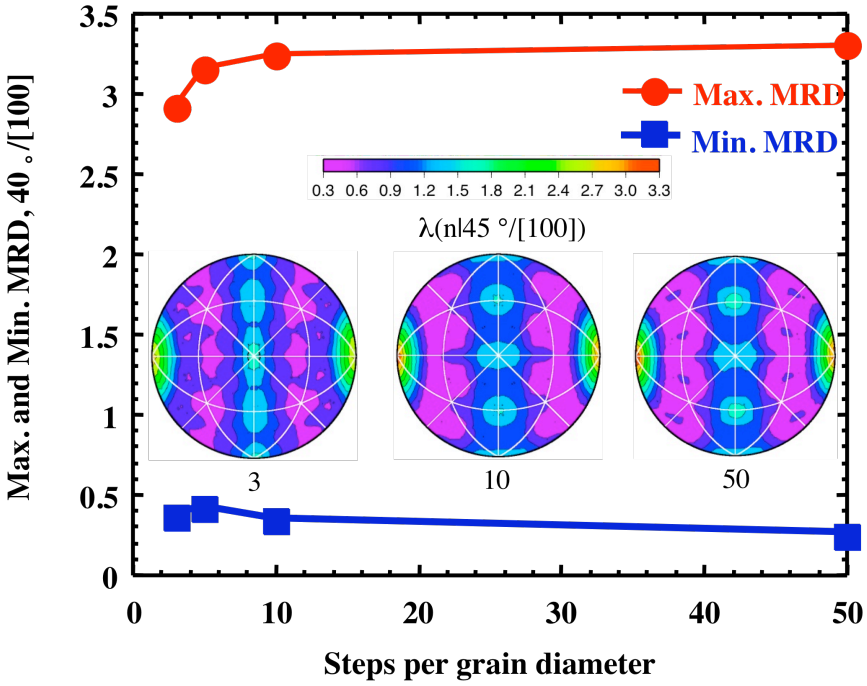

Figure 9. Results from the stereological analysis of simulated data sets with grain boundary traces confined to discrete lattices of different sizes. The circles and squares indicate the maximum and minimum values of the distribution for the 45°/[100] misorientation and the inset shows the grain boundary plane distributions for three of the data sets. The distribution computed from the 10x10 and 50x50 lattices are nearly identical.

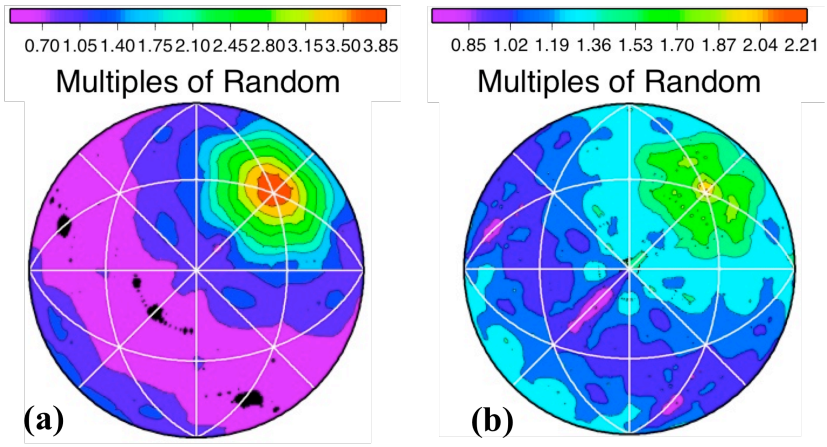

Figure 10. The distribution of grain boundary planes for the Σ3 (60°/[111]) grain boundary in Y_2O_3 computed (a) using the conventional stereology and (b) from 3D data.

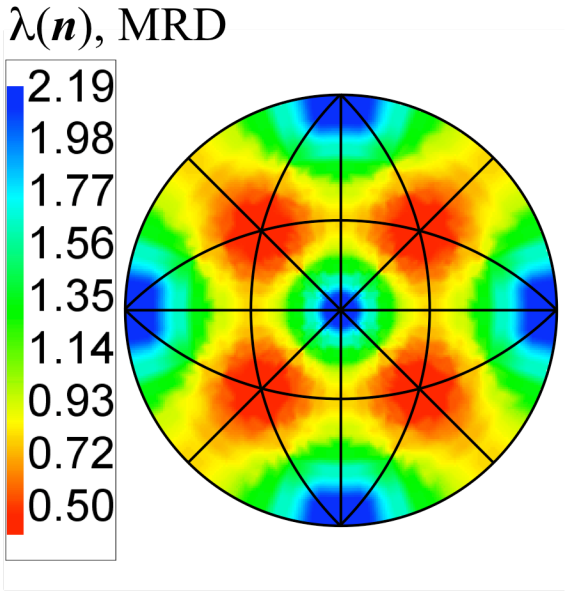

Figure 11. Stereographic projection of grain boundary plane normals from a lightly deformed, wet rocksalt specimem.

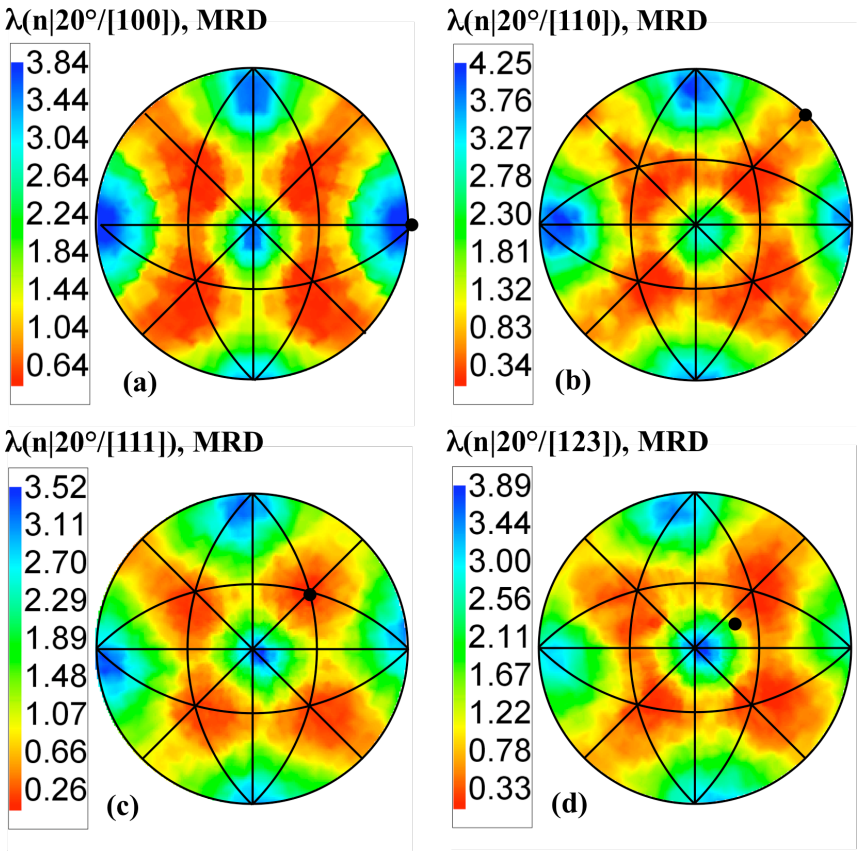

Figure 12. Stereographic projection of grain boundary plane normals from a lightly deformed, wet rocksalt specimen for the (a) 20°/[100], (b) 20°/[110], (c) 20°/[111], (d) 20°/[123] misorientations. In each case, the misorientation axis is marked with a black dot.

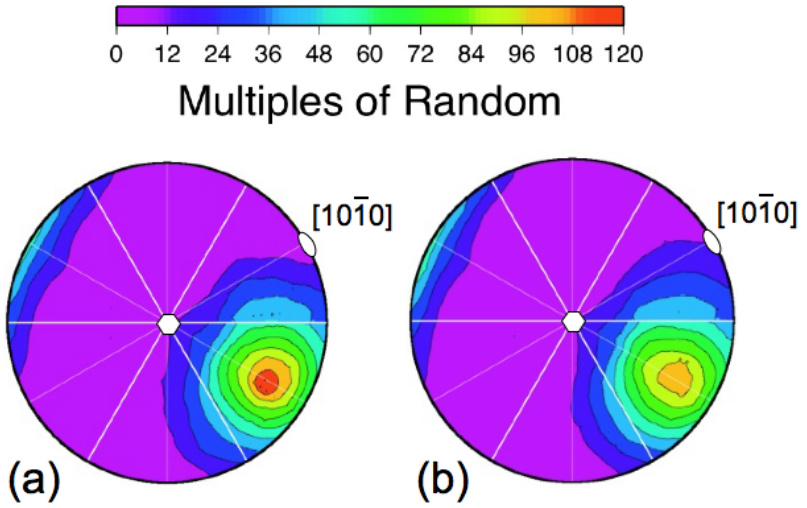

Figure 13. Grain boundary plane distributions for the Σ13b, 57.4°/$[2\bar{1}\bar{1}0]$, grain boundaries in deformed Ti-6%Al-4%V specimens (a) before and (b) after annealing. The [0001] direction is indicated by a hexagon and the $[10\bar{1}0]$ direction is indicated by an oval.

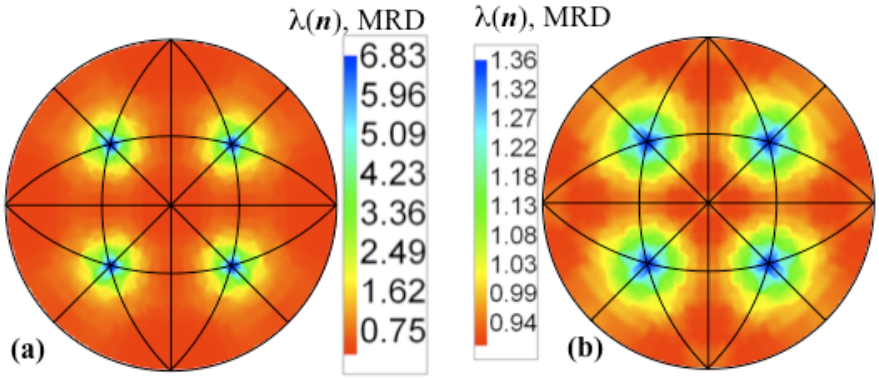

Figure 14. Stereographic projection of grain boundary plane normals from an annealed copper specimen. (a) All grain boundaries included. (b) All grain boundaries other than Σ3.

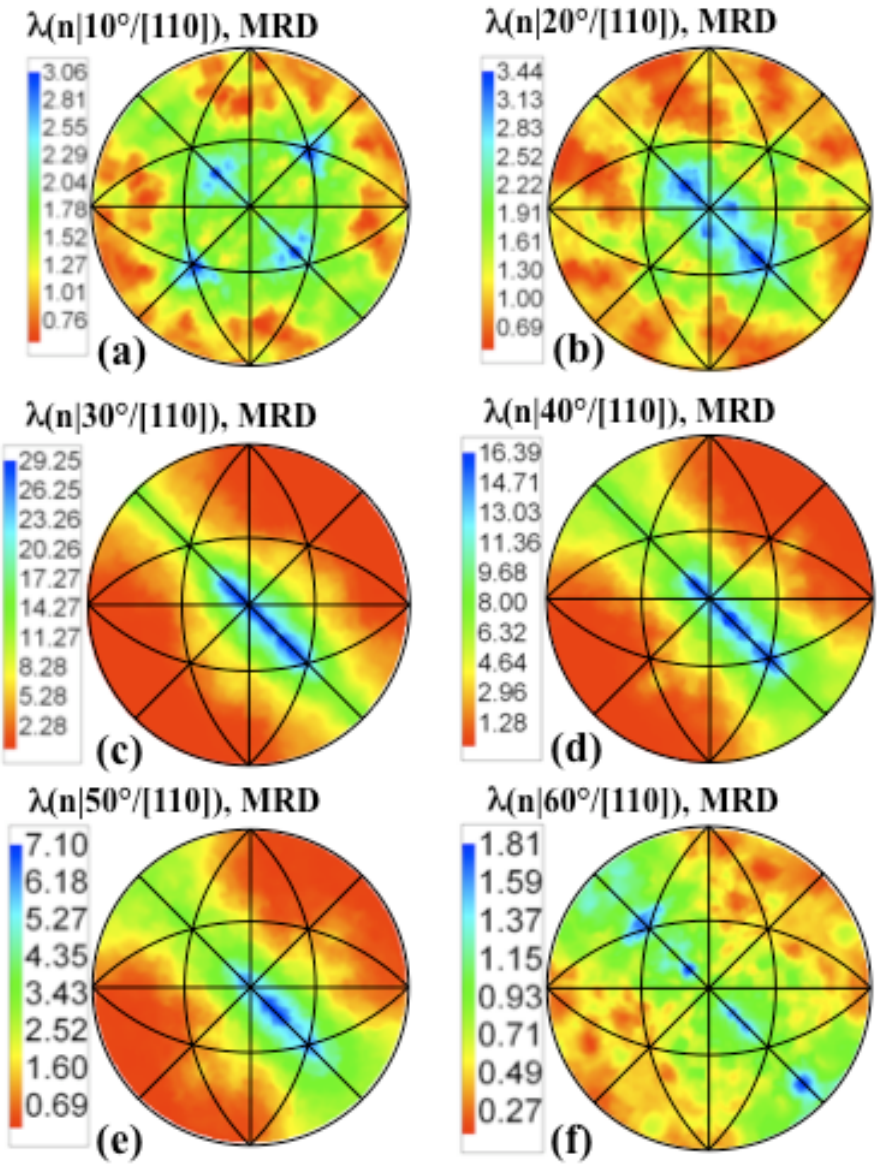

Figure 15. Stereographic projection of grain boundary plane normals from an annealed copper specimen for misorientations about [110], in 10° increments.

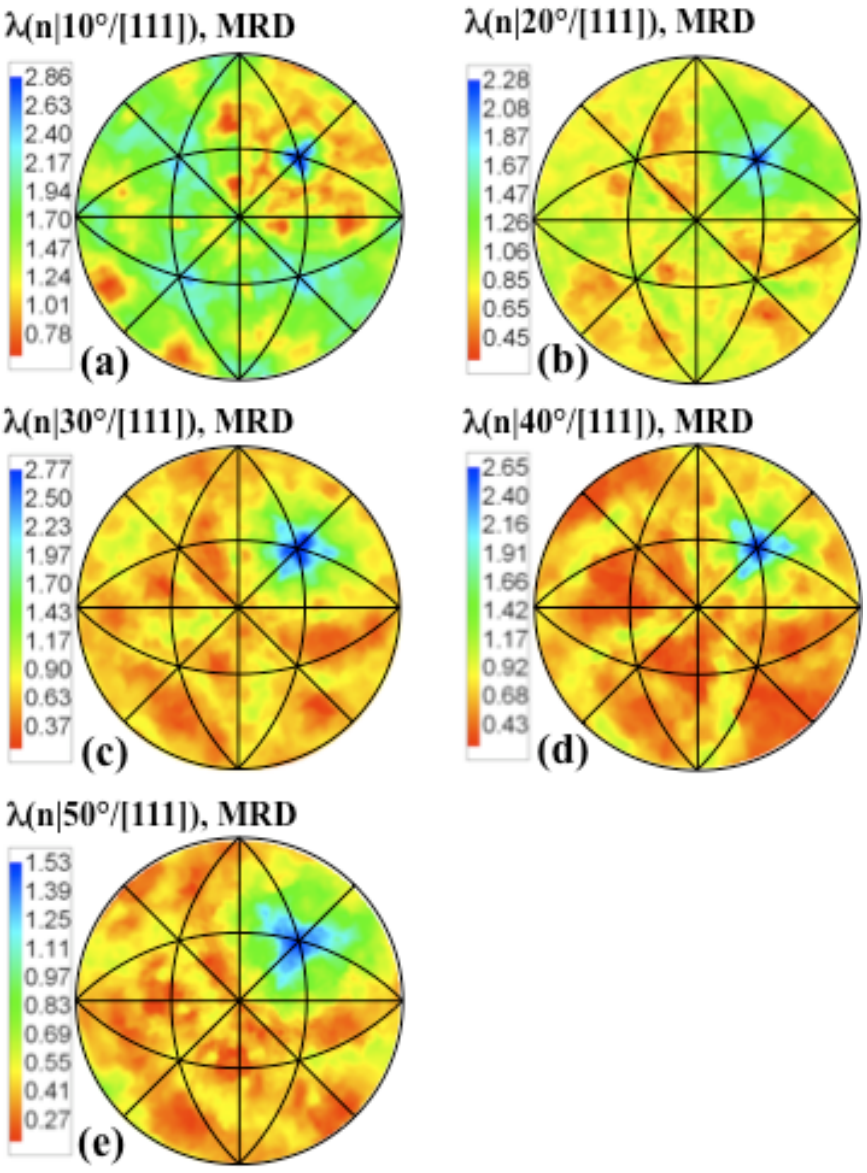

Figure 16. Stereographic projection of grain boundary plane normals from an annealed copper specimen for misorientations on [111], in 10° increments. Σ3 grain boundaries have been excluded from these data and, therefore, the 60° projection is excluded.